Time-frequency distribution of interferograms from a frequency comb in dispersive media

M. G. Zeitouny[1,*], M. Cui[1], A. J. E. M. Janssen[2], N. Bhattacharya[1], S. A. van den Berg[3], and H. P. Urbach[1]

[1]*Technische Universiteit Delft, Lorentzweg 1, 2628 CJ Delft, The Netherlands*
[2]*Technical University Eindhoven, Department EE and EURANDOM, LG-1, P. O. Box 513, 5600 MB Eindhoven, The Netherlands*
[3]*VSL, Thijsseweg 11, 2629 JA Delft, The Netherlands*
[*]*M.Zeitouny@tudelft.nl*

Abstract: We investigate general properties of the interferograms from a frequency comb laser in a non-linear dispersive medium. The focus is on interferograms at large delay distances and in particular on their broadening, the fringe formation and shape. It is observed that at large delay distances the interferograms spread linearly where its shape is determined by the source spectral profile. It is also shown that each intensity point of the interferogram is formed by the contribution of one dominant stationary frequency. This stationary frequency is seen to vary as a function of the path length difference even within the interferogram. We also show that the contributing stationary frequency remains constant if the evolution of a particular fringe is followed in the successive interferograms found periodically at different path length differences. This can be used to measure very large distances in dispersive media.

OCIS codes: (070.4550) Correlators, (070.4790) Spectrum analysis, (120.3180) Interferometry, (320.1590) Chirping, (320.7150) Ultrafast spectroscopy.

References and links

1. D. J. Jones, S. A. Diddams, J. K. Ranka, A. Stentz, R. S. Windeler, J. L. Hall, S. T. Cundiff, Science **288** 635 (2000).
2. R. Holzwarth, Th. Udem, T.W. Hänsch, J. C. Knight, W. J. Wadsworth, and P. St. J. Russell, Phys. Rev. Lett **85**, 2264 (2000).
3. S. T. Cundiff and J. Ye, Rev. Mod. Phys. **75**, 325 (2003).
4. S. A. Diddams, J. C. Bergquist, S. R. Jefferts, C. W. Oates, Science **306**, 1318 (2004).
5. Th.Udem, R.Holzwarth, and T.W.Hänsch, Nature **416**, 233 (2002).
6. L. Hollberg, C. W. Oates, E. A. Curtis, E. N. Ivanov, S. A. Diddams, T. Udem, H. G. Robinson, J. C. Bergquist, R. J. Rafac, W. M. Itano, R. E. Drullinger, and D. J. Wineland, IEEE J. Quant. Elect. **37**, 1502 (2001).
7. J. Ye, H. Schnatz, and L. W. Hollberg, IEEE J. Select. Top. Quant. Elect. **9**, 1041 (2003).
8. J.Ye, Opt. Lett. **29**, 1153 (2004).
9. M. Cui, R. N. Schouten, N. Bhattacharya and S. A. van den Berg, J.E.O.S. - Rapid Publications **3** 08003 (2008)
10. Y. Salvade, N. Schuhler, S. Leveque and S. Le Floch, Appl. Opt. **47**, 2715 (2008) and references therein.
11. K.N.Joo, Y.Kim and S.W.Kim, "Distance measurements by combined method based on a femtosecond pulse laser", Opt. Exp. **16**, 19799 (2008) and references therein.
12. P. Balling, P. Křen, P. Mašika, S. A. van den Berg, Opt. Exp. **17**, 9300-9313 (2009).
13. M. Cui, M. G. Zeitouny, N. Bhattacharya, S. A. van den Berg, H. P. Urbach, and J. J. M. Braat, Opt. Lett. **34**, 1982-1984 (2009).

14. I. Coddington, W. C. Swann, L. Nenadovic and N. R. Newbury, Nature Photonics **3**, 351-356 (2009).
15. J. Lee, Y.-J. Kim, K. Lee, S. Lee, S. Kim, Nature Photonics, Advanced publication online 2010.
16. M. G. Zeitouny, M. Cui, N. Bhattacharya, S.A. van den Berg, A. J. E. M. Janssen, and H.P. Urbach, Phys. Rev. A **82**. 023808 (2010).
17. K.P.Birch and M.J.Downs, Metrologia **31**, 315 (1994).
18. V. A. Borovikov, *Uniform Stationary Phase Method*, IEE Electromagnetic wave series (1994).
19. K. E. Oughstun and N. A. Cartwright, J. Mod. Opt. **52**, 1089 (2005) and references therein.

1. Introduction

Laser sources with carrier-envelope-offset stabilized femtosecond pulses offer the unique advantage of a fixed phase relationship between the pulses emitted by the laser. The long term stability of these sources opens up a whole range of applications in several precision metrology application areas such as precision optical frequency metrology, spectroscopy, and absolute distance measurements [1, 2, 3, 4, 5, 6, 7], to name a few. Measurement of interferograms, or correlations, between pulses gives an insight of the coherence properties of the light source. A normalized correlation from a balanced Michelson interferometer, termed as the autocorrelation, exhibits a peak intensity of unity at exactly equal arms and decaying oscillations as a function of the position of the scanning arm. The autocorrelation is a symmetric function and its Fourier transform yields the power spectral density (PSD) of the laser source according to Wiener-Khintchin theorem. If the interferometer is unbalanced and the measurements are carried out in vacuum, for a frequency comb source, the correlation repeats itself periodically with a maximum coherence when the path length difference between both arms is equal to an integer multiple of the laser cavity length. In this case the correlation patterns remain undistorted and the position of the maximum fringe visibility can be easily and accurately determined.

In the case of distance metrology [8, 9, 10, 11, 12, 13, 14, 15] in air a dispersive medium is placed in the measurement arm. The observed interference patterns, which are cross-correlation patterns, will show distortion when compared to the autocorrelation. Also, the position of the coherence maximum or the brightest fringe will vary as a function of the delay distance. We have shown that [16], even if the medium is homogeneous, the position of the maximum coherence varies non-linearly for short delay distances and linearly for larger delay. In addition, our simulations also show that the correlation patterns are non-linearly broadened at short delay distances and that linear broadening replaces the non-linear broadening at larger distances.

In this work our main focus is on the formation of the fringes and the shape of the cross-correlation patterns for large delay distances. The terms large delay and short delay depend on the extent of distortion in the cross-correlation patterns which in turn is dependent on the properties of the light source and the dispersive medium. We describe the cross-correlation from a mode-locked laser using a discrete model and then extend this to a continuous model, allowing us to derive some dispersion properties of the correlation patterns. In particular, we have shown that the cross-correlation exhibits a non-linear broadening for short delay distances and linear broadening for larger delays. The theoretical results obtained from the developed continuous model are in full agreement with the standard discrete model of the cross-correlation as well as with the measured data. The depth of non-linearity for pulses in dispersive media has been shown to quantitatively depend on the temporal and spectral properties of the emitted light and the dispersion properties of the medium. In this work, using the continuous model of the cross-correlation and the method of the stationary phase we study the behavior of cross-correlation patterns and the frequency content of the constituting optical fringes at large delay distances.

This paper is organized as follows. In Section II a general description of the cross-correlation using the continuous model is presented. In Section III, we use the method of the stationary phase to study the cross-correlation functions and compare it to numerical simulations. Finally, in Section IV a new proposal for distance measurement using the method of stationary phase is

described.

2. Cross-correlation in dispersive media

The starting point of our analysis is provided by a model describing the propagation of plane waves from a pulsed laser along the x-direction. A detailed description of our work can be found in [16]. The frequency spectrum emitted by a mode-locked laser consists of a comb of regularly spaced frequencies $\omega_m = m\omega_r + \omega_0,\ m = 0,1,2,...$ where ω_0 is the common offset frequency and ω_r is the repetition frequency f_r expressed in angular notation $\omega_r = 2\pi f_r = \frac{2\pi}{T_r}$, $T_r = \frac{c}{l_{pp}}$. Here l_{pp} is the cavity length, c is the velocity of light in the medium of the cavity and T_r is the time distance between the pulses. The offset frequency ω_0 is caused by the difference between the group velocity and the phase velocity inside the laser cavity. Both ω_0 and ω_r are stabilized to an atomic clock in most laboratories.

The correlation function can be readily measured experimentally by placing a slow detector at the output of the Michelson interferometer, which can be balanced or unbalanced. A detailed analysis of this function in case of an unbalanced interferometer in presence of a homogenous dispersive medium leads to the following equation [16]

$$\Gamma(X) = \sum_{m=0}^{\infty} S(m\omega_r + \omega_0) \cos\left[(m\omega_r + \omega_0) n(m\omega_r + \omega_0) \frac{X}{c}\right] \tag{1}$$

where $\Gamma(X)$ is the cross-correlation as a function of the delay distance (X), $S(m\omega_r + \omega_0) \equiv$ Power Spectral Density (PSD) and $n()$ is the refractive index of the dispersive medium. Equation (1), which is a discrete representation of the correlation function, shows good agreement with the experimental results but is unable to provide a physical explanation of some properties of the cross-correlation function such as the the shift of the position of the maximum coherence, broadening effects and shape of the cross-correlation function. A continuous model was therefore developed for a better understanding of the problem.

We can rewrite the cross-correlation as [16]

$$\Gamma(X) = \frac{T_r}{2} \sum_{\ell=-\infty}^{\infty} h_X\left(\bar{n}\frac{X}{c} + \ell T_r\right), \tag{2}$$

using the Poisson summation formula. Here the subscript X in h_X is a parameter denoting the delay distance. This analysis is in the regime where inspite of the broadening the extent of the cross-correlation function is still smaller than the laser cavity length or the interpulse distance. This series expression, Eq. (2), for $\Gamma(X)$ reduces to at most a single term when $h_X(t)$ has a support length $\leq T_r$. The limitation posed by this for the case of propagation in air is discussed in a subsequent section. From a physical point of view, the integer ℓ denotes the multiple of the laser cavity length at a given delay distance X and ℓT_r is the propagation time of a pulse in "vacuum". In the case where $X > 0$ the integer ℓ must be negative. Defining the time variable (t) as

$$t \equiv \bar{n}\frac{X}{c} \pmod{T_r}, \tag{3}$$

allows us to write the cross-correlation function as an integral given by

$$h_X(t) = \frac{1}{\pi}\int_0^{\infty} S(\omega + \omega_0) \cos\left\{(\omega + \omega_0)\left[n(\omega + \omega_0) - \bar{n}\right]\frac{X}{c} + \omega_0 \bar{n}\frac{X}{c} + \omega t\right\} d\omega. \tag{4}$$

From Eq. (4) we see that for any arbitrary delay distance X, independent of the laser cavity length $2\pi c/\omega_r$, a cross-correlation pattern $h_X(t)$ can be obtained by varying the time delay (t)

where $-T_r/2 \leq t \leq T_r/2$. In practice, this time (t) is obtained by setting up a scanning short arm of one laser cavity length. For numerical comparisons, both $h_X(t)$ and $\Gamma(X)$, are normalised to unity.

Using the Wiener-Khintchin theorem and a quadratic dispersive medium $k(\omega+\omega_0) = \alpha\omega^2 + \beta\omega + \gamma$ for large delay distances, we can write [16]

$$h_X(t) = \frac{R}{2\pi}\sqrt{\frac{\pi}{2\alpha X}}\cos\left[\gamma X - f_X^2(t) + \theta\right]\int_{-\infty}^{\infty} dt_0 h_{X=0}(t_0)]\cos\left[\frac{f_X(t)}{\sqrt{\alpha X}}t_0\right]. \tag{5}$$

Here, $f_X(t)$ is defined as $f_X(t) = -\left(\beta X - \bar{n}\frac{X}{c} + t\right)/(2\sqrt{\alpha X})$, R and θ are radial and angular parameters which are functions of $f_X(t)$ [16]. These results have allowed us to define a particular function $\zeta(X)$ by

$$\zeta(X) = \frac{\tau_c}{\sqrt{(4\alpha X)}} = \frac{\tau_c}{\sqrt{\frac{2}{c}\left[2\frac{dn(\omega)}{d\omega} + \omega\frac{d^2n(\omega)}{d\omega^2}\right]_{\omega=\omega_0} X}} \tag{6}$$

Using this function defined the Non-linear Dispersion Depth ($\mathscr{D}$) of a given pulse in a particular dispersive medium. The parameter $\mathscr{D}$ is given as

$$\mathscr{D} = \frac{3}{2}\sqrt[3]{\frac{\tau_c^2}{\alpha}} \tag{7}$$

Equation (7) shows the effective distance of non-linear dispersion effects on cross-correlations obtained from a light source having a coherence time τ_c and a carrier frequency ω_c propagating in a refractive medium with a group delay dispersion α at ω_c. Short delay and large delay distances can be defined using $\mathscr{D}$.

2.1. Typical characteristics of cross-correlations at large delay distances

In this section, we numerically analyze cross-correlation patterns for delay distances larger than $\mathscr{D}$. For standard air we have previously shown [16] that $\mathscr{D} = 30$ m. Our simulations were performed for standard air using the measured laser source spectrum [13]. The typical parameters for our Ti:Sapphire based frequency comb are as follows. The central frequency of the comb is $\omega_c = 2.3254 \times 10^{15}$ rad/s, corresponding to a wavelength of 810 nm in vacuum, the bandwidth is typically $\Delta\omega \approx 5 \times 10^{14}$ rad/s, which correspond to a pulse width of $\Delta x \approx 12\ \mu m$ and a pulse duration of 40 fs. The frequency offset is typically $\omega_0 \approx 113 \times 10^7$ rad/s and the repetition frequency is $\omega_r = 6.28 \times 10^9$ rad/s, corresponding to a cavity length $l_{pp} = 30$ cm and period $T_r \approx 1$ns. The frequencies ω_0 and ω_r are synchronized to a cesium clock. The spectral content of the initial pulse is the main input for the numerical model. Using the corrected updated Edlén's equation [17] for the refractive index of air, 8×10^4 spectral lines fitted to the profile of the spectrum of the laser, are propagated and then recombined to form correlation patterns.

In this numerical example the delay distance X has been taken to be long enough, 120 meters, so that the correlation patterns are only observed to be linearly broadened. Three fringes are picked up from this correlation pattern and further analysed. The cross-correlation is shown in Fig. 1.a where the vertical lines indicate the positions of the fringes we investigate. The fringe pattern is obtained by varying the time delay t around a delay distance $X = 120$ m. At each small delay the frequency content of the interfering fields will be constantly in phase or out of phase depending on t. We have chosen to analyze the cosine of the phase factor from Eq. (4). For each small delay scan one fringe the cosine of the phase function has been plotted. A 3-D plot can be obtained for each analyzed fringe showing the value of the cosine of the phase

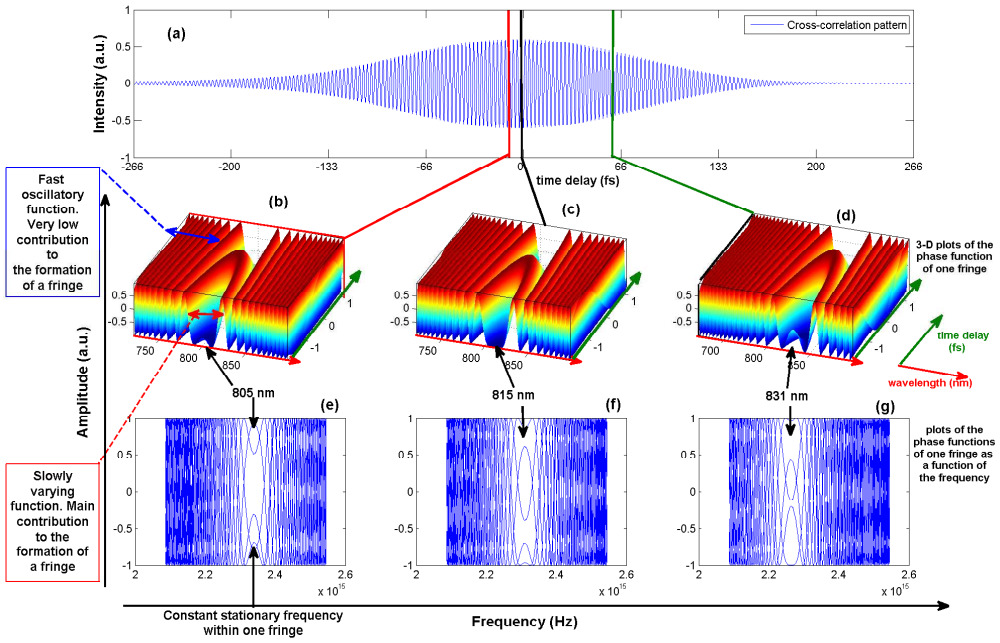

Fig. 1. Behaviour of the phase function for various fringes within one correlation. (a) Cross correlation for a propagation distance $X = 120$ m. The three lines select three different fringes from the cross-correlation pattern. (b,c,d) The corresponding 3-D plots of the cosine of the phase function of the three selected fringes are shown as a function of the wavelength and the scanning time t. (e,f,g) The cosine of the phase function of the three selected fringes as a function of frequency for five intensity values in each fringe.

as a function of the time delay (t) and the frequencies (or the wavelength) of the optical field. These plots are shown in Fig. 1.(b,c,d). The plots show that within one fringe the cosine of the phase function has either fast or slow oscillations as a function of the frequency. Using this oscillating function in Eq. (4), where $S(\omega+\omega_0)$ is a slowly varying term, the integral transform is small. The integral will approach zero as the number of oscillations increases, Riemann-Lebesgue lemma. Thus this relatively high oscillatory part will have a minor contribution to the formation of the interference fringe. Only when the cosine of the phase function is slowly varying the contribution to the integral will be important. The plots analyzing the fringes show that the slowly varying part is always at a specific frequency for a particular fringe. In Fig. 1.(e,f,g) we plot the cosine of the phase function for each fringe as a function of the frequency. Five such samples at different intensity points of the fringe are plotted on top of each other. It is clearly seen that, for a given fringe, the position of the stationary frequency remains constant on the frequency-axis and changes only in value when t changes. Between different fringes, the stationary frequency varies, depending on the fringe position in the correlation pattern.

We study the evolution of the cosine of the phase function from Eq. (4) as a function of the distance in Fig. 2. We pay particular attention to the behaviour of this function at the brightest fringe of the cross-correlations. For short distances the cosine of the phase function is slowly oscillating. In this case we have a large contribution from the whole frequency band of the source. As the distance increases, the cosine of the phase function becomes highly oscillating and the formation of the fringe depends on a small frequency bandwidth which is

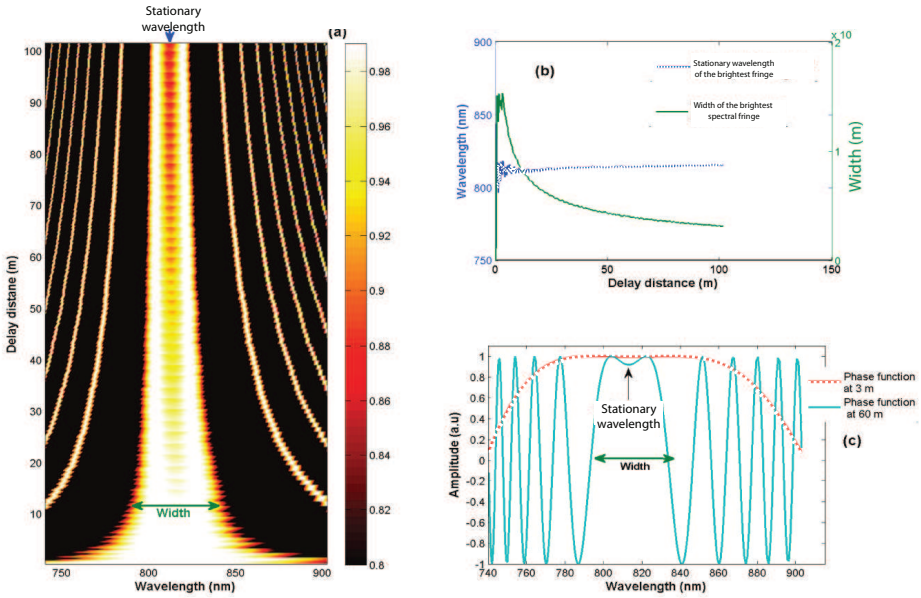

Fig. 2. (a) Analysis of the cosine of the phase function at the brightest fringe of the correlation pattern for various delay distances ranging up to 100 m in air. (b) Wavelength (green, continuous) and width (blue, dotted) of brightest fringe as a function of delay distance. (c) Cross-sections from the cosine of the phase function shown in (a) illustrating the phase function at 3 m (red, dotted) and 60 m (blue, continuous).

the slowly oscillating part. The width of the slowly oscillating part converges as the distance increases. The central frequency of the slowly oscillating part is constant and becomes a dominant frequency after reaching a delay distance larger than $\mathscr{D}$ which is more than 30 m in standard air.

2.2. Limit of the validity of the continuous model in standard air

In this section we calculate the maximum pulse propagation distance for which the correlations can be analyzed using the continuous model. The dispersive medium under investigation is standard air. It is essential that the cross-correlation $\Gamma(X)$ in Eq. (2) contains one significant term only. So that $\Gamma(X)$ is simply proportional to $h_X(t)$ where t is defined by Eq. (3). We rewrite Eq. (4) as

$$h_X(t) = \frac{1}{\pi}\mathrm{Re}\left\{\int_0^\infty S(\omega+\omega_0)\exp\left[i\left(\bar{n}\frac{X}{c}\xi(\omega+\omega_0)+\omega t\right)\right]d\omega\right\}, \tag{8}$$

where we have defined $\xi(\omega+\omega_0) = (\omega+\omega_0)\left[\frac{n(\omega+\omega_0)}{\bar{n}}-1\right]$. Therefore, for $X=0$, $h_X(t)$ reduces to

$$h_{X=0}(t) = \frac{1}{2\pi}\int_{-\infty}^{\infty} S(\omega+\omega_0)\exp(i\omega t)d\omega \tag{9}$$

Recalling that $S(\omega+\omega_0)$ is the power spectral density of a single pulse. Using the Wiener-Khintchin theorem, where the autocorrelation of the pulse has a time duration τ, we get

$$\begin{aligned} h_X(t) &= \mathrm{Re}\left\{\frac{1}{\pi}\int_{-\infty}^{\infty} h_{X=0}(t)\left[\int_0^{\infty}\exp\left(-i\omega t_1 + i\bar{n}\frac{X}{c}\xi(\omega+\omega_0)+i\omega t\right)d\omega\right]dt_1\right\} \\ &= \mathrm{Re}\left[\frac{1}{\pi}\int_{-\infty}^{\infty} h_{X=0}(t_1)g_X(t-t_1)dt_1\right], \end{aligned} \tag{10}$$

where $g_X(s)=\int_0^{\infty}\exp\left[i\omega s+i\bar{n}\frac{X}{c}\xi(\omega+\omega_0)\right]d\omega$. Thus h_X is obtained as the real part of the convolution of $h_{X=0}$ and $\frac{1}{\pi}g_X$. The range of the time interval s for which $g_X(s)$ is non-negligible is to be determined. The time interval range t for which $h_X(t)$ is non-negligible is then just a little bit larger in size than the corresponding range for g_X. To obtain the time interval range for g_X, the stationary points in the integrand of g_X need to be determined. We assume $\xi(\omega)=\omega n_0(\omega)$ where $n_0=\frac{n(\omega)}{n}-1=\varepsilon_0\phi(\tau\omega)$. Here ε_0 is a number of the order 10^{-7} and $\phi(\eta)$ is a smooth function such that both $\phi(\eta)$ and $\phi^{'}(\eta)$ are of the order of unity. Now $g_X(s)$ can be written as

$$\begin{aligned} g_X(s) &= \int_0^{\infty}\exp\left[i\omega s+i\bar{n}\frac{X}{c}(\omega+\omega_0)\varepsilon_0\phi(\tau(\omega+\omega_0))\right]d\omega \\ &= \exp(-i\omega_0 s)\frac{1}{\tau}\int_{\tau\omega_0}^{\infty}\exp(i\eta s^{'})\exp\left(ib^{'}\eta\phi(\eta)\right)d\eta, \end{aligned} \tag{11}$$

where $s^{'}=\frac{s}{\tau}$ and $b^{'}=\bar{n}\frac{X}{c}\frac{\varepsilon_0}{\tau}$. In the above equation, Eq. (11), a stationary point occurs in the integral for the set of $s^{'}$ which obeys the condition

$$\frac{\partial}{\partial\eta}\left[\eta s^{'}+b^{'}\eta\phi(\eta)\right]=s^{'}+b^{'}\left[\phi(\eta)+\eta\phi^{'}(\eta)\right]=0 \tag{12}$$

where $\eta\in[\tau\omega_0,\infty]$. Therefore $s^{'}\in\left\{b^{'}\left[\phi(\eta)+\eta\phi^{'}(\eta)\right]\mid\eta\in\mathrm{R}\right\}$. The set of $s^{'}$ has the same size at the set of $b^{'}$ since $\phi(\eta)+\eta\phi^{'}(\eta)$ is of the order of unity. The average refractive index $\bar{n}$ of air in the near infrared region is 1.00027. Therefore $b^{'}\tau$ has a size of the order $b^{'}\tau=\frac{\bar{n}\varepsilon_0}{c}X=\frac{1}{3}10^{-15}X$. This gives us a range for the set s contained in the interval of length T_r when $X\leq 3.10^{15}T_r=3.10^6$ m.

This analysis gives an approximate indication of the size of the set where g_X is non-negligible, but for the relevant cases that $X\leq 1000$ km it seems that we can safely assume that the series in Eq. (2), that uses samples of h_X at distances T_r apart, has only one significant term. In any case, these distances are beyond the coherence length of present day laser systems but maybe relevant in the future.

In the next section we will show that for large delay distances, particularly larger than $\mathscr{D}$, an asymptotic method can be used to derive the equation of the cross-correlation function. Results from this asymptotic method and Eq. (5), which uses the continuous model, will be compared to each other. Using this, a simple method for absolute distance metrology is proposed.

3. Stationary phase approximation of the cross-correlation function

To study the correlation functions and their properties for large delay distances, we define large delay as the distance for which the correlation patterns are only linearly broadened. We have shown by numerical simulations and experimental measurements that the shape of the cross-correlation converges to a particular profile for large delay distances. In air, we were able to

study this for correlations patterns up to 200 m, where the numerical results agreed reasonably well with the experiments [16].

To simulate the correlation formation in air under experimental conditions we used the standard discrete model. In spite of the reasonable agreement that has been obtained between numerical and experimental results, we were not able to explain the physical origin of the shape convergence and disappearance of the effect of chirp at large delay distances. To understand the formation of the cross-correlation patterns at large distances we extended the discrete model to a continuous model. This enabled us to write the cross-correlation as an integral, Eq. (4) instead of a series. Using this integral we now try to study the quasi-asymptotic formation of cross-correlation patterns.

The cross-correlation in Eq. (4) is expressed as an integration of a slowly varying function, $S(\omega+\omega_0)$, multiplied by an oscillatory phase factor. The stationary phase method is an appropriate mathematical tool to study the asymptotic behaviour of this model [18]. We rewrite Eq. (4) as

$$h_X(t) \quad = \quad \frac{1}{2\pi}\int_0^\infty S(\omega+\omega_0)\left\{\exp[i\phi(\omega)]+\exp[-i\phi(\omega)]\right\}d\omega \tag{13}$$

where $\phi(\omega)=k(\omega+\omega_0)X-\omega\bar{n}\frac{X}{c}+\omega t$ and $k(\omega+\omega_0)=(\omega+\omega_0)n(\omega+\omega_0)/c$. The phase $\phi(\omega)$ is stationary when $\frac{d}{d\omega}\left[k(\omega+\omega_0)X-\omega\bar{n}\frac{X}{c}+\omega t\right]=0$ or, equivalently, when $\frac{dk}{d\omega}=\frac{\bar{n}}{c}-\frac{t}{X}$. Solutions to this differential equation yield dominant frequencies $\omega_{dom}(X,t)$ for a given X and t, where $t\in\left\{\bar{n}\frac{X}{c}-k^{(1)}(\omega)X \mid \omega\in \mathrm{R}\right\}$. Here $k^{(1)}$ denotes the first derivative of the $k(\omega)$ vector. If we expand $\phi(\omega)$ in a Taylor series about ω_{dom} and neglect terms of order higher than $(\omega-\omega_{dom})^2$, we obtain $\phi(\omega)\sim k(\omega_{dom}+\omega_0)X-\omega_{dom}\bar{n}\frac{X}{c}+\omega_{dom}t+\frac{X}{2}\frac{d^2k}{d\omega^2}(\omega-\omega_{dom})^2$. This phase expansion yields the first order stationary phase approximation of Eq. (13). This general class of oscillatory integrals, with polynomially growing phase functions, also has a solution where higher-order stationary phase approximation can be calculated. The asymptotic solution of Eq. (13) using only the first and the second order stationary phase approximation is given by

$$h_X(t)\simeq\frac{1}{\pi}\left\{C_1X^{-1/2}\cos\left[\phi(\omega_{dom})+\sigma\frac{\pi}{4}\right]+C_2X^{-3/2}\cos\left[\phi(\omega_{dom})+\sigma\frac{3\pi}{4}\right]\right\} \tag{14}$$

where the coefficients C_n are given below. With $\sigma=\mathrm{sign}[\phi^{(2)}(\omega_{dom})]$ where $\phi^{(n)}$ is the n^{th} derivative of $\phi(\omega)$ evaluated at the frequency ω_{dom}, the first two coefficients of the asymptotic series are given by [18]

$$C_1=\sqrt{\frac{2\pi}{|\phi^{(2)}(\omega_0)|}}S(\omega_{dom}+\omega_0) \tag{15}$$

and

$$C_2=\frac{\sqrt{\pi/2}}{|\phi^{(2)}|^{3/2}}\left[S^{(2)}-\frac{\phi^{(3)}S^{(1)}}{\phi^{(2)}}-\frac{\phi^{(4)}S}{4\phi^{(2)}}+\frac{5(\phi^{(3)})^2S}{12(\phi^{(2)})^2}\right]. \tag{16}$$

Here $S^{(n)}$ are the n^{th} derivative of $S(\omega+\omega_0)$. Then, the first order asymptotic approximation, where $C_2=0$, of the cross-correlation function is given as by

$$h_X(t)\simeq\frac{1}{\pi}S(\omega_{dom}+\omega_0)\sqrt{\frac{2\pi}{X\left|\frac{d^2k}{d\omega^2}\right|_{\omega=\omega_{dom}}}}\cos\qquad\left[k(\omega_{dom}+\omega_0)X-\omega_{dom}\bar{n}\frac{X}{c}+\omega t+\sigma\frac{\pi}{4}\right] \tag{17}$$

The second order approximation is given by

$$h_X(t)\simeq\frac{1}{\pi}\left\{C_1X^{-1/2}\cos\left[\phi(\omega_{dom})+\sigma\frac{\pi}{4}\right]-\sigma C_2X^{-3/2}\sin\left[\phi(\omega_{dom})+\sigma\frac{\pi}{4}\right]\right\}. \tag{18}$$

When a and b are real, we can write $a\cos x - b\sin x = \mathscr{R}\cos(x+\vartheta)$. In this case $\mathscr{R}$ and ϑ are given by $\mathscr{R} = \sqrt{\frac{C_1^2}{X} + \frac{C_2^2}{X^3}}$ and $\tan\vartheta = -\sigma\frac{C_2}{XC_1}$. Finally, the second order approximation can be written as

$$h_X(t) \quad \simeq \quad \frac{1}{\pi}\mathscr{R}\cos\left[k(\omega_{dom}+\omega_0)X - \omega_{dom}\overline{n}\frac{X}{c} + \omega t + \sigma\frac{\pi}{4} + \vartheta\right] \tag{19}$$

From the above expression we see that the first order stationary phase approximation is the leading contributor. In optical media, as well as in air, the dispersion relation can generally be limited to its quadratic approximation [19]. In this case, terms arising due to higher order stationary phase approximations have minor contribution to the formation of the cross-correlation function. In the subsequent analysis we use the first and the second order terms and neglect the rest. From Eq. (17) we can see that the dominant term results in the envelope of the cross-correlation being determined by the spectral profile $S(\omega+\omega_0)$. This is in agreement with the previous experimental and numerical simulation [16], where we observe shape convergence of cross-correlation functions at large delay distances. The equation also shows that the term inside the cosine depends linearly on ω_{dom}. Thus, with increasing delay distance the cross-correlation functions will spread linearly.

We compare various simulated correlations using Eq. (1) and their corresponding asymptotic functions using the stationary phase approximations from Eq. (14) in Fig. 3. We refer to the cross-correlation from Eq. (1) and the one from Eq. (14) as the exact and the asymptotic cross-correlations respectively. We start our comparison using the first order stationary phase method. Numerical results for 100 m delay distance in air are shown in Fig. 3.a. At the center of the interferogram a good overlap between the exact and the asymptotic correlation has been obtained. An analysis of the wings of the interferogram show a fringe mismatch. A better

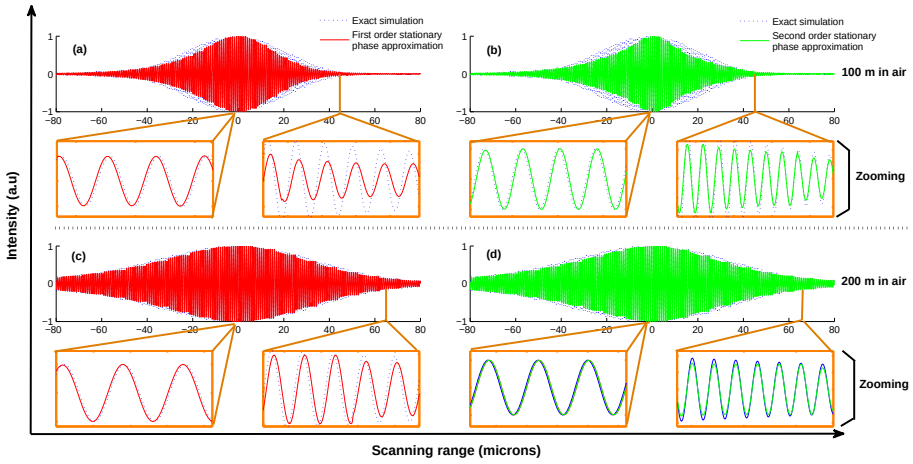

Fig. 3. Comparison between exact and asymptotic cross-correlations for 100 and 200 m in air using the first and the second order stationary phase method. (a) Exact simulation (blue, dotted) compared to first order asymptotic calculation (red, continuous) for 100 m propagation in air. (b) Exact simulation (blue, dotted) compared to second order asymptotic calculation (green, continuous) for 100 m propagation in air. (c) Exact simulation (blue, dotted) compared to first order asymptotic calculation (red, continuous) for 200 m propagation in air. (d) Exact simulation (blue, dotted) compared to second order asymptotic calculation (green, continuous) for 200 m propagation in air.

overlap has been obtained for a delay distance of 200 m and shown in Fig. 3.c. This problem

of shape matching between the exact and the asymptotic correlations can be alleviated using higher-order stationary phase approximation. Here we only show the improvements using the second-order stationary phase. It is clearly seen that for higher order stationary phase approximation the shape of the asymptotic pattern shows a better agreement with the exact correlation. More importantly, for distance measurement purposes, the position of the central fringe of the asymptotic correlations has not shown any shift in comparison to the exact simulations.

We found that for larger distances, fringe patterns can be described by particular frequencies. In Fig. 4 we show the frequency content of a correlation pattern simulated for a delay of 200 m in air. The top figure shows the spectral distribution of the laser source. The bottom figure

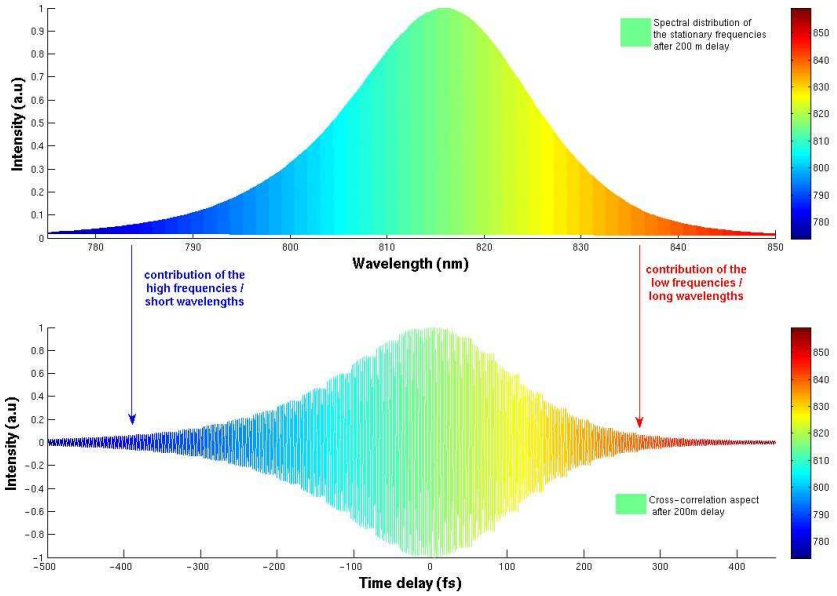

Fig. 4. (top) Spectral distribution of the stationary frequencies after 200 m propagation in air. (bottom) Frequency distribution inside a cross-correlation after 200 m propagation in air.

shows the cross-correlation function simulated using the first-order stationary phase method. The color indicates the frequency content ranging from 780 to 850 nm. It is clearly seen that the stationary frequencies change within a given cross correlation depending on the fringe order. In addition, the shape of the envelope of the cross-correlation follows the shape of the spectral distribution as it was demonstrated in this section. Using this approximation greatly reduces the computational time when simulating the cross-correlation functions as can be seen when Eq. (17) and Eq. (1) are compared. As an example, the spectrum of the Ti:Saphirre frequency comb contains 10^5 frequencies. By using a scanning short arm with 10^4 steps, one has to compute a grid of $10^5 \times 10^4$ elements in order to obtain the final results. This can be simply reduced to a vector of 10^4 components by using the cross-correlation equations from the stationary phase method since we can associate one dominant frequency to each scanning step.

4. Stationary Phase Absolute Distance Metrology

In the previous section we observed that the analysis of cross-correlation patterns becomes simpler for large delay distances, when the stationary phase approximation can be applied. Each fringe in the cross-correlation is formed by its unique dominant frequency and the cross-correlation broadens only linearly. In this section we will show that by accurate knowledge of the spacing between two fringes of different frequencies we can determine the absolute distance of the measurement arm in dispersive media at large delays.

We would like to compare Eq. (5) and Eq. (17). Both equations are only valid for large delay distances and are calculated for a quadratic dispersive medium. In the result obtained from the first order stationary phase approximation as shown in Eq. (17, the cross-correlation has the envelope of the power spectral density of the laser source, $S_(\omega_{dom}+\omega_0)$, at the dominant frequencies ω_{dom}. The envelope of the cross-correlation from Eq. (5) is given by the following integral

$$\int_{-\infty}^{\infty} h_{X=0}(t_0)\exp\left[i\left(\frac{t+\beta X-\bar{n}X/c}{2\alpha X}\right)t_0\right]dt_0. \tag{20}$$

The exponential can be written as $\exp[i\omega_p(X,t)t_0]$, where $\omega_p(X,t)=(t+\beta X-\bar{n}X/c)/(2\alpha X)$ is a particular angular frequency depending on the delay distance and the scanning time t. Therefore we can replace the above integral with $S[\omega_p(X,t)]$ where we have used the Wiener-Khintchin theorem. Here $S[\omega_p(X,t)]$ is the power spectral density at the particular angular frequencies $\omega_p(X,t)$. Thus we can see that the envelope of the cross-correlation patterns in quadratic dispersive media is determined by the shape of the PSD of the laser source. We observe a linear dependence between the stationary frequencies, $\omega_p(X,t)$, and the scanning time t. In the regime where the extent of the cross-correlation function is smaller than the laser cavity length, the value of t is given by Eq. (3).

Consider the case where the output of the unbalanced Michelson interferometer was analyzed with a spectrometer, we would then measure modulated spectra instead of cross-correlation patterns. If we perform two independent measurements at the same distance X but at two different scanning positions of the short scanning arm, t_1 and t_2 respectively. From the expression for $\omega_p(X,t)$ we obtain

$$\begin{aligned}
&\begin{cases} \frac{t_1}{X}=\frac{\bar{n}}{c}-\beta+2\alpha\omega_p(X,t_1) \\ \frac{t_2}{X}=\frac{\bar{n}}{c}-\beta+2\alpha\omega_p(X,t_2) \end{cases} \\
&\Rightarrow \frac{t_2-t_1}{X}=2\alpha\left[\omega_p(X,t_2)-\omega_p(X,t_2)\right]
\end{aligned} \tag{21}$$

The time lag ($\Delta t=t_2-t_1$) can be measured by simply noting the piezo displacement (Δx), where $\Delta t=\frac{\Delta x}{c}$. The spectrometer would record the particular or dominant frequencies at two different positions of the scanning piezo. Hence, the unknown distance X is determined by

$$X=\left|\frac{\Delta x}{2c\alpha\left[\omega_p(X,t_1)-\omega_p(X,t_2)\right]}\right| \tag{22}$$

This method is quite simple. It requires the measurement of two stationary frequencies at two different positions. The accuracy of this method depends on the resolution of the spectrometer and the sensitivity of the scanning element (piezo) in the short arm. This can be a subject for future experiments at large delay distances as a fast method for absolute distance measurements

5. Conclusion

The continuous model of cross-correlations allows us to understand many aspects of the formation of correlation patterns after propagation in dispersive media. The cross-correlation patterns

are subject to non-linear broadening at short path length differences and linear broadening at larger path length differences. For path length differences beyond the non-linear dispersion depth, the method of stationary phase was used to study the correlation patterns. It shows that the shape of the cross-correlation patterns at large delay distances is determined by the source spectral profile, though the cross-correlation will continue spreading linearly. It was also observed that each intensity point of the correlation pattern is formed by the contribution of one dominant stationary frequency. This stationary frequency is seen to vary as a function of the path length difference within the correlation pattern. We also show that the contributing stationary frequency remains constant if the evolution of a particular fringe is followed in the successive cross-correlation patterns found periodically at different delay distances for the long arm. Using this property a method of measuring very large distances has been proposed.

6. Acknowledgements

The authors would like to thank Omar El Gawhary for extensive discussions. The authors gratefully acknowledge J. J. M. Braat for his thoughtful comments on the manuscript. This work is part of the Industrial Partnership Programme (IPP) Metrology with Frequency Comb Laser (MFCL) of the Stichting voor Fundamenteel Onderzoek der Materie (FOM), which is supported financially by Nederlandse Organisatie voor Wetenschappelijk Onderzoek (NWO). The IPP MFCL is co-financed by VSL, TNO and ASML. The research within this work is also a part of EURAMET joint research project and has received funding from the European Community's Seventh Framework Programme, ERA-NET Plus, under Grant Agreement No. 217257.